AIAA 79-1709R

Fuel-Conservative Guidance System for Powered-Lift Aircraft

Heinz Erzberger* and John D. McLean*
NASA Ames Research Center, Moffett Field, Calif.

A technique is described for the design of fuel-conservative guidance systems and is applied to a system that was flight tested on board NASA's augmentor wing jet STOL research aircraft. An important operational feature of the system is its ability to rapidly synthesize fuel-efficient trajectories for a large set of initial aircraft positions, altitudes, and headings. This feature allows the aircraft to be flown efficiently under conditions of changing winds and air traffic control vectors. Rapid synthesis of fuel-efficient trajectories is accomplished in the airborne computer by fast-time trajectory integration using a simplified dynamic performance model of the aircraft. This technique also ensures optimum flap deployment and, for powered-lift STOL aircraft, optimum transition to low-speed flight. Also included in the design is accurate prediction of touchdown time for use in four-dimensional guidance applications. Flight test results have demonstrated that the automatically synthesized trajectories produce significant fuel savings relative to manually flown conventional approaches.

Nomenclature

D = drag force, lb
d_b, d_f = distance of backward and forward integration, respectively
d_c = cruise distance, ft
d_h = length of ground track from initial to final position of aircraft, ft
E = energy, ft
$\dot{E}_n$ = energy rate, ft/s
$\dot{E}_{n\max}, \dot{E}_{n\min}$ = maximum and minimum available energy rate, respectively, ft/s
F, G = perturbation state and control distribution matrices, respectively
g = acceleration of gravity, ft/s^2
H_f, H_i = final and initial ground headings of aircraft, deg
h = altitude, ft
h_f, h_i = final and initial altitudes of aircraft, respectively, ft
K = feedback gain matrix
$k_{\phi y}, k_{\phi \dot{y}}$ = lateral error and error rate feedback gains
L = lift force, lb
$\dot{S}$ = speed along ground track, ft/s
T = thrust force, lb
t = time, s
u = perturbation control vector
$\bar{u}_1, \bar{u}_2, \bar{u}_3, \bar{u}_4$ = two-dimensional unit vectors
u_c = aircraft control vector
V_a = airspeed, ft/s or knots
V_{af}, V_{ai} = final and initial airspeeds of aircraft, respectively, ft/s or knots
V_w = wind speed in direction of ground track, knots
W = aircraft weight, lb
x = perturbation state vector
X_f, X_i = final and initial X coordinates of aircraft, respectively, ft
Y_f, Y_i = final and initial Y coordinates of aircraft, respectively, ft
α = angle of attack, deg
γ = ineritial flight-path angle, deg
γ_a = aerodynamic flight-path angle, rad or deg
$\Delta \dot{V}_a$ = airspeed rate correction due to wind shear, ft/s^2
Δ_y = crosstrack error, ft
$\Delta_{\dot{y}}$ = crosstrack error rate, ft/s
δ_f = flap angle, deg
$\delta_{f\max}$ = maximum flap angle, deg
ϵ = fraction of energy rate used for changing speed
θ_c = command pitch angle, deg
ν = vectored thrust angle, in degrees of nozzle angle
π = throttle setting, in percent rpm
σ = fraction of available energy rate
ϕ_c, ϕ_r = commanded and reference bank angles, respectively, deg

Presented as Paper 79-1709 at the AIAA Guidance and Control Conference, Boulder, Colo., Aug. 6-8, 1979; submitted March 7, 1980; revision received Aug. 14, 1980. This paper is declared a work of the U.S. Government and therefore is in the public domain.

*Research Scientist. Member AIAA.

Introduction

In the past, terminal area guidance system design for aircraft has concentrated primarily on automatic glide-slope tracking, flare, and touchdown. During recent years, designs have been developed to provide automatic guidance along curved and decelerating approach paths.[1] This increased capability was made possible through the integration of digital computers into the flight guidance system. However, even in the more advanced designs, automatic guidance is limited to a few prestored three-dimensional (3-D) flight paths, as in Ref. 1. While the ability to fly complex prestored trajectories is essential, it cannot give optimum performance under actual terminal area operating conditions, as shall be explained.

First, a prestored trajectory cannot optimize fuel consumption or a similar performance measure under actual operating conditions. Optimum trajectories depend significantly on aircraft gross weight, wind and temperature profiles, and the initial state of the aircraft. These variables cannot be predicted with the required precision prior to takeoff. To prestore optimum trajectories for each of the conditions likely to be encountered would result in an impossible large memory requirement. Therefore, prestored trajectories must necessarily represent a compromise in performance.

Second, in existing systems, the pilot must fly the aircraft manually from its current position to the starting point of the trajectory. This flight segment is known as the capturing maneuver. Three-dimensional curved trajectories can be difficult to capture manually, and, if the trajectory also includes a specification of landing time, as is the case in four-dimensional (4-D) guidance, the capturing maneuver cannot be done by the pilot without computer assistance. Therefore, the capturing maneuver, because of its variability, can only be generated by onboard trajectory synthesis.

Third, aircraft in high-density airspace are usually controlled by air traffic control vectors and during this period cannot follow a prestored flight path. Synthesis of a trajectory can only begin after the aircraft has received its final vector and has been cleared for approach. But the initial position of the aircraft at that time varies between approaches; thus, trajectories require onboard synthesis.

An initial design of a 4-D guidance system embodying the concept of onboard trajectory synthesis, including an advanced capture law, was previously developed and flight tested onboard a conventional aircraft equipped with advanced avionics.[2] In the design described here, a new algorithm for generating horizontal capture trajectories has been implemented and vertical and speed profiles are synthesized using simplified aero/propulsion performance models of the aircraft. This method results in profiles that are more fuel efficient than those of earlier design. Design of the control law for tracking the synthesized trajectory is based on the linearized perturbation guidance approach. Since the perturbation equations are aircraft configuration dependent, gain scheduling is used in the feedback law.

The Augmentor Wing Jet STOL Research Aircraft (AWJSRA) was chosen as the test vehicle for this concept. This type of powered-lift aircraft is highly cost-sensitive to operational procedures in the terminal area. It also exemplifies particularly well the unique problems of powered-lift aircraft, namely, high fuel consumption in the STOL mode; dependence of both lift and drag on thrust; and an excess of controls over the minimum number needed to determine path and speed. These factors suggest that trajectory optimization could greatly increase the operational efficiency of the aircraft. Implementation of this concept was facilitated by the existing installation of an advanced avionics system onboard the aircraft.

Energy Rate Model and Selection of Reference Controls

An energy rate model of aircraft performance has been found to yield a compact and sufficiently accurate representation of performance for terminal area trajectory synthesis. In this section, a performance model based on energy rate is derived and then applied to determine the optimum reference controls for synthesizing trajectories.

Consider the standard expression for energy rate written as

$$\frac{dE}{dt} = \frac{(T-D)V_a}{W} \tag{1}$$

where

$$E = h + (1/2g)V_a^2 \tag{2}$$

with constraint $L = W$ (Ref. 3). It is assumed throughout this paper that flight-path angles are small such that $\cos\gamma_a \approx 1$ and $\sin\gamma_a \approx \gamma_a$. Furthermore, it is assumed that flight-path angle rates are so small that their effect on lift is negligible. Differentiation of Eq. (2) with respect to time gives an equivalent expression for energy rate:

$$\frac{dE}{dt} = \frac{dh}{dt} + \frac{1}{g}V_a\frac{dV_a}{dt} \tag{3}$$

Equations (1) and (3) can be nondimensionalized by dividing them both by V_a. The resulting quantity on the left side, $(1/V_a)(dE/dt)$, is defined as the normalized energy rate $\dot{E}_n$, or energy rate for short. By using the relation $(dh/dt) \approx V_a\gamma_a$, the two relations for $\dot{E}_n$ become

$$\dot{E}_n = (T-D)/W \tag{4}$$

$$\dot{E}_n = \gamma_a + \frac{1}{g}\frac{dV_a}{dt} \tag{5}$$

with constraint $L = W$.

Equation (4) specifies the energy rate as a function of the difference between thrust and drag, subject to the constraint that lift equals weight. Thrust and drag are, in turn, functions of the controls producing forces in the flight-path direction; namely, throttle π, flap angle δ_f, nozzle angle ν (vectored thrust), and angle of attack α. Equation (5) determines the relationship between flight-path angle and deceleration for the energy rate calculated from Eq. (4). Equation (5) indicates that, in particular, a given energy rate may be utilized to fly at flight-path angle γ_a with constant airspeed, or to fly at zero flight-path angle with acceleration dV_a/dt. An infinity of other combinations of γ_a and dV_a/dt can also be chosen to yield the same energy rate. This makes possible a simplifying dichotomy in the trajectory synthesis; namely, at any time the desired energy rate is selected first by choice of appropriate controls and then the linearly related quantities of γ_a and dV_a/dt are selected to generate the specifics of the flight path.

Since the STOL aircraft studied in this paper has four controls to achieve a specified energy rate and to maintain lift equal to weight, there is an excess of two controls over the minimum number needed for a simultaneous solution to Eq. (4) and the constraint $L = W$. These two extra degrees of freedom in the controls are exploited to minimize power setting and, therefore, fuel flow at every energy rate. This optimization problem is restated in equivalent form as the maximization of energy rate for a given power setting:

$$\dot{E}_n(\pi) = \max_{\nu,\alpha,\delta_f}(T-D)/W \tag{6}$$

$$\text{Constraint:}\quad L(\pi,\nu,\alpha,\delta_f) = W$$

The maximization must obey various inequality constraints on the controls:

$$-10.5\ \text{deg} \le \alpha \le 19.5\ \text{deg}$$

$$6\ \text{deg} \le \nu \le 100\ \text{deg}$$

$$5.6\ \text{deg} \le \delta_f \le \delta_{f\max}(V_a) \quad \text{[flap placard]}$$

In addition, a lift or maneuver margin must be satisfied at every point to guarantee sufficient normal force for changing the flight path. Pilots familiar with this aircraft specify that at least 0.4 g of normal acceleration must be attainable at any time by an increase in the angle of attack alone.

The use of Eq. (6) results in the selection of the controls that yield the maximum attainable energy rate at each thrust

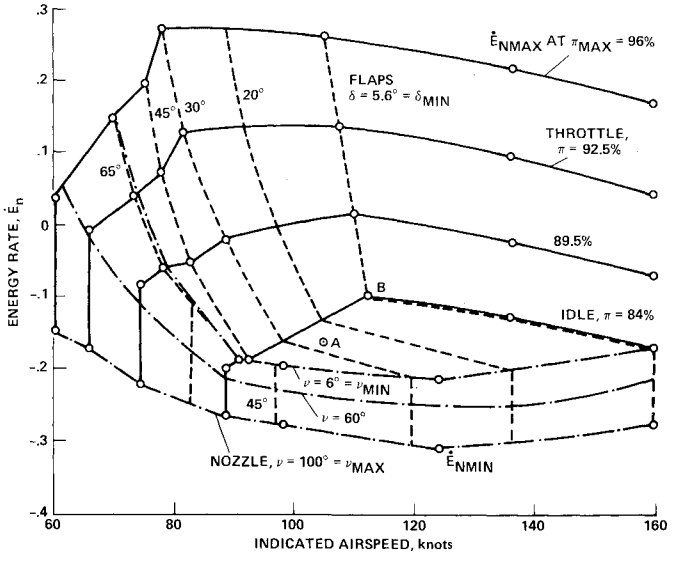

Fig. 1 Energy rate diagram for STOL aircraft: $W = 38{,}000$ lb, sea level 59°F.

setting. This insures the efficient use of thrust at any energy rate that requires more than the minimum thrust. But energy rates more negative than those attainable by Eq. (6) are also of interest. Such negative energy rates must occur at the greater of the minimum or idle thrusts required by the maneuver margin. At a particular airspeed, a decrease in the energy rate below the minimum attained through Eq. (6) can be effected by increasing the vectored thrust angle ν and/or the flap angle δ_f. The third control, angle of attack α, is needed to satisfy the constraint $L = W$. The two degrees of freedom in the controls can be exploited to minimize noise exposure along the ground track. Noise under the aircraft is known to increase as the nozzles producing the vectored thrust are turned downward. Therefore, a further decrease in energy rate is achieved by first increasing flap angle until it reaches its limit or placard value and only then by increasing nozzle angle.

The result of applying these procedures to the AWJSRA is shown in Fig. 1 for a weight of 38,000 lb, sea-level altitude, and standard temperature. The figure gives the envelope of energy rate vs indicated airspeed with throttle, flaps, and vectoring nozzle as parameters. Angle of attack is not plotted to avoid cluttering the figure. At any airspeed, the $\dot{E}_{n\max}$ and $\dot{E}_{n\min}$ curves define the range of permissible energy rates. The optimum controls for a given airspeed and energy rate are determined by interpolation between contours of constant controls. For example, at an airspeed of 105 knots and $\dot{E}_n = -0.17$, the optimum controls are found to be $\delta_f = 26$ deg, $\nu = 6$ deg, and $\pi = 84\%$ (point A, Fig. 1). Angle of attack (not shown) is 8.4 deg. Maximum energy rate with minimum thrust occurs at 112 knots (point B) and corresponds approximately to $(L/D)_{\max} = 10$.

It should be noted that the force-producing controls in this experimental STOL aircraft have unusual characteristics that account for the relative complexity of Fig. 1. Throttle affects both lift and drag at all speeds, but the effect on lift is greatest in the STOL regime below about 80 knots. The thrust magnitude produced by the vectoring nozzle, referred to as the hot thrust, is also controlled by the throttle and accounts for about 60% of the total thrust produced by the two engines. The remaining 40% of the thrust, which is the cold thrust produced by the fans, energizes the augmentor wing to increase lift at STOL speeds.

The relationship between the controls and the energy rate is revealed more clearly in Fig. 2 at the example airspeed of 105 knots. Many such plots at various airspeeds would be required to illustrate the complete dependence of the controls on energy rate. As the energy rate decreases below its maximum value of 0.28, throttle decreases nearly linearly until idle throttle is reached. In this interval, flaps increase only slightly, while nozzle angle remains at minimum and angle of attack increases. At more negative energy rates, flaps become the dominant control until they reach the placard value of 40 deg at this airspeed. Angle of attack decreases sharply as flap angle increases. Finally, nozzle angle increases toward its maximum value of 100 deg as the energy rate decreases toward its negative limit of -0.3.

In the flight implementation of the algorithm, four diagrams, as shown in Fig. 1, are utilized: two for sea-level altitude at weights of 38,000 and 48,000 lb, and two others for 5000-ft altitude at similar weights. Experience indicates that these provide sufficient data to adequately interpolate the controls. Each diagram requires 124 words of memory in the airborne computer. The small circles in Fig. 1 indicate the locations of points that are stored. The energy rate data are also corrected for deviations from the standard temperature profile. Correction is done by computing a thrust setting corrected for temperature deviations.

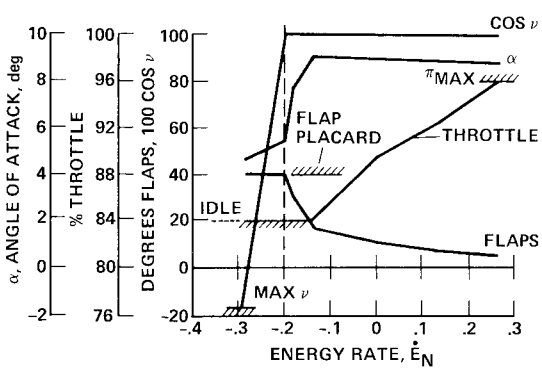

Fig. 2 Optimum controls as function of energy rate at 105 knots: $W = 38{,}000$ lb, sea level 59°F.

Synthesis of Complete Profiles

In the preceding section the criteria of fuel conservation and noise reduction were used to determine the four reference controls of throttle, nozzle angle, flap angle, and angle of attack as functions of the energy rate. This approach replaced the problem of selecting four control variables with the simpler problem of selecting a single, equivalent variable, namely, the energy rate. In this section, we make use of the energy-rate variable in generating efficient terminal area trajectories.

The problem of terminal area trajectory synthesis can be stated as the specification of rules for flying an aircraft with initial state vector $[X_i, Y_i, h_i, H_i, V_{ai}]$ to a final state vector $[X_f, Y_f, h_f, H_f, V_{af}]$. To be of practical interest, such rules must generate efficient and flyable trajectories connecting various initial and final state vectors. By specifying a performance criterion such as fuel consumption, we can fit this problem into the framework of optimal control theory. However, the difficulty of solving an optimal control problem characterized by a five-element state vector makes this approach computationally impractical for in-flight implementation. Following Ref. 4, we have adopted the simplifying procedure of separating the synthesis problem into two essentially independent problems.

The first problem consists of synthesizing the horizontal or 2-D trajectory. References 4 and 5 give algorithms for computing near-minimum-distance 2-D trajectories as a sequence of an initial constant radius turn, straight flight, and a final constant radius turn, where the turn radii are chosen so as to avoid exceeding a specified maximum bank angle at the maximum groundspeed encountered in each turn. The algorithm used in this onboard computer implementation is based on a simplified derivation which resulted in a significant reduction in computing time compared with the methods given in the references. The derivation can be found in the Appendix. Figure 3 illustrates two of the four types of horizontal trajectories that can occur; the two not shown differ only in the orientation of the turns. The algorithm

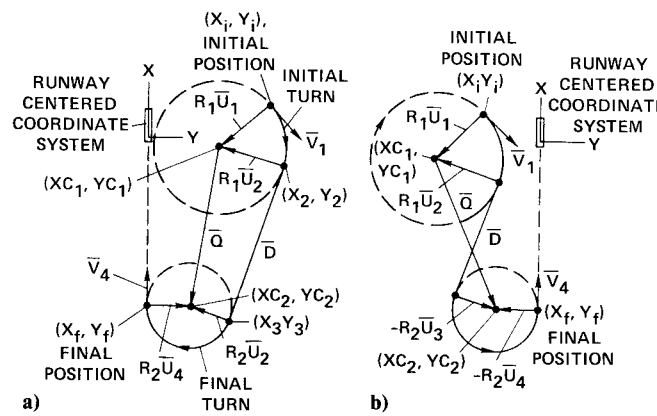

Fig. 3 Examples of minimum distance, constant turn radius, horizontal capture trajectories to a capture point P_f on final approach: a) turns in same direction; b) turns in opposite direction.

computes all feasible trajectories, of which there are at least two and at most four, and chooses the one with the shortest path length. Note that the terminal point lies on an extension of the runway centerline and that the final heading angle is equal to the runway heading. The final point should be chosen as close as possible to the touchdown point consistent with safe operational practice. For a STOL aircraft, the minimum distance is about 1 n.mi.

The second problem, solved after the horizontal trajectory has been computed, consists of synthesizing efficient speed and altitude profiles which match the initial and final speeds and altitudes V_i, h_i, and V_f, h_f, respectively.

The horizontal distance of the trajectory d_h, a known quantity computed in the previous step, adds a third boundary condition to be satisfied by the profiles. While this three-state optimal control problem is much simpler to solve than the original five-state problem, it is still too complex for onboard-computer implementation. A simpler algorithm was, therefore, developed that generates near-optimum speed-altitude profiles by matching the general characteristics of optimum fuel and noise trajectories studied in Refs. 6 and 7, respectively. We briefly explain the rationale for this algorithm with reference to descent, which is the most difficult case.

It was found in Ref. 6 that the descent portion of a minimum-fuel descent trajectory is characterized by a delay in the start of the energy decrease as long as possible, consistent with meeting end constraints of speed and altitude. Furthermore, the energy change consists initially of descent to the final altitude at near-constant indicated airspeed followed by deceleration in level flight. Most of the energy change takes place at minimum throttle, as one might expect for minimum fuel flight. Minimum-noise descent profiles computed in Ref. 7 are similar in that they also delay the start of energy decrease as long as possible, but approach the final altitude in a steep descent to maximize the aircraft's altitude above the ground near the runway. This means that the deceleration to the final airspeed takes place before the start of descent or during the early portion of the descent. Thus, the two types of descent profiles differ primarily in the way they proportion the use of available energy rate to decrease altitude and airspeed.

To facilitate the synthesis of such profiles, a family of decreasing (and by extension, increasing) energy profiles, which include the two types described as special cases, is defined by two parameters, σ and ϵ. The first parameter, σ, selects the fraction of minimum/maximum available energy rate, $\dot{E}_{n\min}$, ($\dot{E}_{n\max}$) to be used for decreasing/increasing energy. The values of $\dot{E}_{n\min}$ and $\dot{E}_{n\max}$ can be read from Fig. 1 at each indicated airspeed. The second parameter, ϵ, determines the fraction of the selected energy rate to be used for deceleration/acceleration. Then, for particular choices of σ and ϵ, the energy rate, airspeed, flight-path angle, altitude, and horizontal distance are computed as follows:

$$\dot{E}_n = \sigma \dot{E}_{n\min} \qquad (0 \le \sigma \le 1) \tag{7}$$

$$\dot{V}_a = g\epsilon \dot{E}_n \qquad (0 \le \epsilon \le 1) \tag{8}$$

$$\gamma_a = (1-\epsilon)\dot{E}_n \tag{9}$$

$$\dot{h} = V_a \gamma_a \tag{10}$$

$$\dot{S} = V_a \cos\gamma_a + V_w \tag{11}$$

where V_w is the along-track component of windspeed. Note that Eqs. (7-9) are consistent with Eqs. (4) and (5) for all values of σ and ϵ. Decreasing/increasing energy profiles are generated by integrating Eqs. (8), (10), and (11) for particular choices of σ and ϵ.

To illustrate the effect of the parameter ϵ on the descent/deceleration profiles, assume $\dot{E}_n = -0.13$, independent of speed, and let the airspeed to be achieved at touchdown be 100 ft/s. To achieve the desired boundary conditions, Eqs. (8), (10), and (11) are integrated in backward time starting with the speed and altitude at touchdown. The resulting airspeed and altitude profiles are plotted as a function of distance to touchdown in Fig. 4 for $\epsilon = 1, 0.5, 0.0$. The profile for $\epsilon = 1$ is seen to approximate the minimum fuel, for $\epsilon = 0$, the minimum noise descent and for $\epsilon = 0.5$, a compromise between fuel and noise minimization.

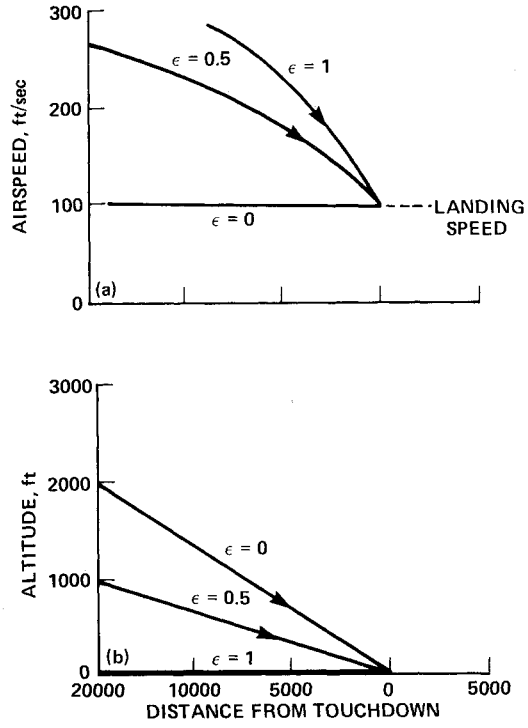

Fig. 4 Effect of ϵ on speed and altitude profiles, with $\dot{E}_n = -0.13$.

To minimize fuel consumption or noise, changes in energy should be made at maximum rate when the aircraft enters the powered-lift region of 90 knots and below. This is accomplished by setting σ to unity and thereby following the $\dot{E}_{n\min}$ contour during descent and deceleration. However, for the aircraft under study this can yield energy rates too negative for safe operation. A limit less than one is also necessary to reserve energy rate for perturbation control. A practical upper limit on σ is about 0.9 for the AWJSRA. In the flight implementation, the two profile parameters are keyboard entries that allow the pilot to choose values appropriate for each landing approach. In addition, the pilot can specify the maximum deceleration and descent angles via keyboard entry. The maximum safe deceleration for this aircraft is limited to about 0.06 g by the maximum rate of which flaps can be extended. The synthesis algorithm is configured to decrease σ below its limit if that is necessary to satisfy these constraints.

The backward time integration described above generates an increasing (in backward time) energy profile starting at the desired final speed and altitude. To complete the synthesis of the descent trajectory, we still need rules for matching this profile to the initial speed and altitude of the aircraft. The freedom of the aircraft to maneuver in altitude is restricted by air traffic control as well as passenger comfort considerations. Thus, as an aircraft approaches a terminal area, it is generally not allowed to climb above its initial approach altitude for the purpose of optimizing the approach trajectory. The aircraft must hold this altitude until starting the final descent. However, while flying at altitude h_i, it may change to a new airspeed, V_{at}, called the terminal area speed, which can be higher or lower than the initial speed V_{ai}. Unless specified by the pilot via keyboard entry, it is chosen to

minimize fuel use per unit distance, and is 140 knots for this aircraft (it would be 220-250 knots for conventional jet transports).

The various rules contained in the preceding two paragraphs can now be combined to yield the complete algorithm. The synthesis begins with the backward time integration from final conditions h_f, V_{af} using the specified σ and ϵ. If the altitude reaches its target value of h_i before the airspeed reaches its target value of V_{at}, we set $\epsilon = 1$ and then continue the backward time integration until the airspeed has also achieved its target value. When setting $\epsilon = 1$, the flight-path angle is forced to zero and the energy rate is used entirely for accelerating (in backward time) toward V_{at}. On the other hand, if the airspeed reaches its target value before the altitude does, we set $\epsilon = 0$. This stops the airspeed change and uses the energy rate entirely for increasing the altitude toward its target value of h_i. When the second and last variable reaches its target value, we set $\sigma = 0$, i.e., $\dot{E}_n = 0$, thus completing the backward time integration. Next, we begin a forward time integration to get the distance required to change speed from V_{ai} to V_{at} with $\epsilon = 1$. Let the distances for the backward and forward integrations be d_b and d_f, respectively. A valid trajectory has been generated if the cruise distance d_c, computed from

$$d_c = d_h - d_b - d_f \tag{12}$$

is nonnegative, i.e., $d_c \geq 0$. If d_c is negative, the synthesis has failed because the aircraft is too close to the capture point P_f.

Figure 5 illustrates the various segments of an approach trajectory synthesized by the algorithm. As before, we assume for simplicity that $\dot{E}_n = -0.13$, a constant. Other parameters defining the problem are indicated in the figure. Note that the initial descent at $\gamma_a = -7.5$ flattens to $\gamma_a = -3.75$ to allow the aircraft to decelerate. The reference controls for this trajectory can be interpolated from Fig. 1.

The airspeed deceleration is corrected for known wind shears, which are computed from a knowledge of $V_w(h)$, if available. The wind shear correction factor is

$$\Delta\dot{V}_a = -(\mathrm{d}V_w/\mathrm{d}h)\, V_a \gamma_a$$

and is added to the right side of Eq. (8) to obtain the corrected airspeed rate. Furthermore, the reference controls are corrected for the effect of the bank angle used in flying a turn by interpolating the controls with lift equal to an aircraft weight multiplied by the load factor $1/\cos\phi$. Integration step size varies during synthesis. During decelerations or accelerations it is 1 s, while during altitude changes at fixed speed it is 5 s. Total time for synthesizing a complete trajectory consisting of a horizontal trajectory similar to the ones shown in Fig. 3 and a speed/altitude profile similar to the one in Fig. 5 is about 2 s on the particular airborne computer used in the flight tests. When the trajectory synthesis is time-shared with navigation and other necessary computations, the computing time increases to about 6 s.

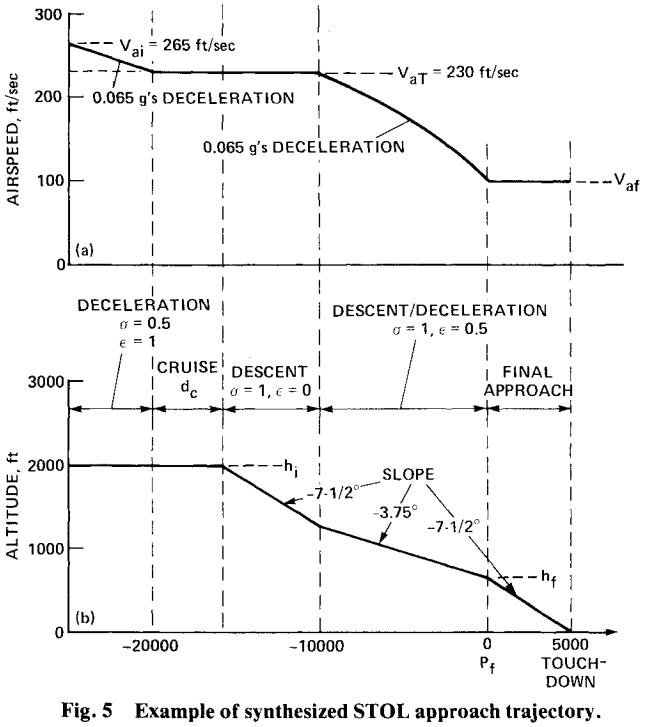

Fig. 5 Example of synthesized STOL approach trajectory.

Perturbation Guidance Law

Perturbations of the aircraft states from the reference states are used in the guidance law to generate perturbation controls which are added to the reference controls in order to null errors in airspeed, altitude, and crosstrack position. The feedback states in the guidance law also include crosstrack error rate and flight-path angle, as well as the integrals of airspeed and altitude errors. The latter two are used to reduce speed and altitude bias errors caused by inaccuracies in the stored energy rate data and errors in the estimates of wind and temperature profiles.

The controls are throttle, nozzle, pitch, and roll angles. Flaps are not used as perturbation controls because of their relatively low rate limit and an operational constraint that flap motion be monotonic during an approach. The flap command is simply the reference value at each ground track position limited to the placard value at the current airspeed.

Lateral perturbation control is essentially uncoupled from the longitudinal mode and is accomplished through a roll-angle command to the roll-command autopilot. This command is of the form

$$\phi_c = \phi_r + k_{\phi y}\Delta y + k_{\phi \dot{y}}\Delta\dot{y}$$

where ϕ_r is the reference roll angle, and Δy and $\Delta\dot{y}$ are the crosstrack error and error rate, respectively. The two gains were chosen to provide a well-damped response and control activity compatible with the noise characteristics of the navigation system.

Longitudinal perturbation control for correcting airspeed and altitude errors is difficult because the reference controls generated by the energy rate schedule of Fig. 1 often lie on a constraint boundary and therefore cannot be perturbed freely in both directions. The two controls that are often constraint-limited during a fuel-conservative approach are throttle π,

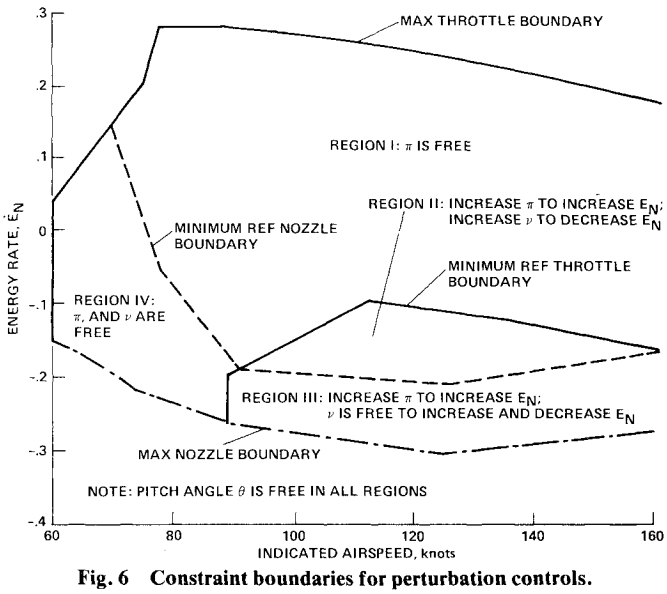

Fig. 6 Constraint boundaries for perturbation controls.

and nozzle angle ν. Some insight into this problem can be obtained using data from the energy rate schedules. Figure 6 shows the energy rate envelope from Fig. 1 with the minimum reference nozzle and throttle constraint boundaries. These boundaries divide the envelope into four regions: I, where ν cannot be reduced; II, where neither π nor ν can be reduced; III, where π cannot be reduced; and IV, where π and ν are free to move in either direction. The combinations of controls available for increasing and decreasing $\dot{E}_n$ in each region are indicated in the figure. Note that in region I, the nozzle could be used as a additional control variable for decreasing energy rate. However, this variable is not used because throttle and pitch provide adequate control of flight-path errors in this region. In region IV, the minimum reference throttle is above idle and is determined by the maneuver margin constraint. At each airspeed in this region the negative throttle perturbation that can be added to the reference throttle to yield the commanded throttle is limited to -2% for safety reasons. Positive and negative throttle perturbations are further limited so that the commanded throttle π_c falls into the engine operating range, $84\% \leq \pi \leq 96\%$.

The perturbation equations and the perturbation control law can be written in state vector notation as

$$dx/dt = Fx + Gu \qquad u = Kx$$

where

$$x = (\Delta V, \Delta\gamma, \Delta h, \int \Delta V dt, \int \Delta h dt)^T$$

$$u = (\Delta\pi, \Delta\theta, \Delta\nu)^T$$

The delta quantities are the perturbations from reference values, i.e., $\Delta V = V_a - V_{ar}$, etc., where V_a is the aircraft and V_{ar} the reference true airspeed, respectively. The commanded controls are the sum of reference and perturbation controls:

$$u_c = (\pi_r + \Delta\pi, \theta_r + \Delta\theta, \nu_r + \Delta\nu)$$

For a powered-lift STOL aircraft, such as the one used for these flight tests, the values of F and G are strongly dependent upon airspeed and energy rate and are thus time-varying along a trajectory. Quadratic optimal synthesis[8] would therefore yield time-varying gain matrices that are also functions of the reference trajectory. But it is neither practical nor necessary to implement a complex, reference-trajectory-dependent gain matrix in order to achieve adequate control system performance in this case.

The design procedure employed here began by first computing optimum gain matrices at various operating points in the control region diagram (Fig. 1) using fixed values of F and G. The analysis of these gain matrices showed the strongest dependence on airspeed, reference nozzle angle, and reference flaps. Sensitivity of the closed-loop eigenvalues to changes in several of the gains was low, allowing those to be set to zero or held constant throughout the operating region. It was possible to fit the variable gains with relatively simple functions of reference airspeed, nozzle angle, and flap angle. This method resulted in the following gain matrix:

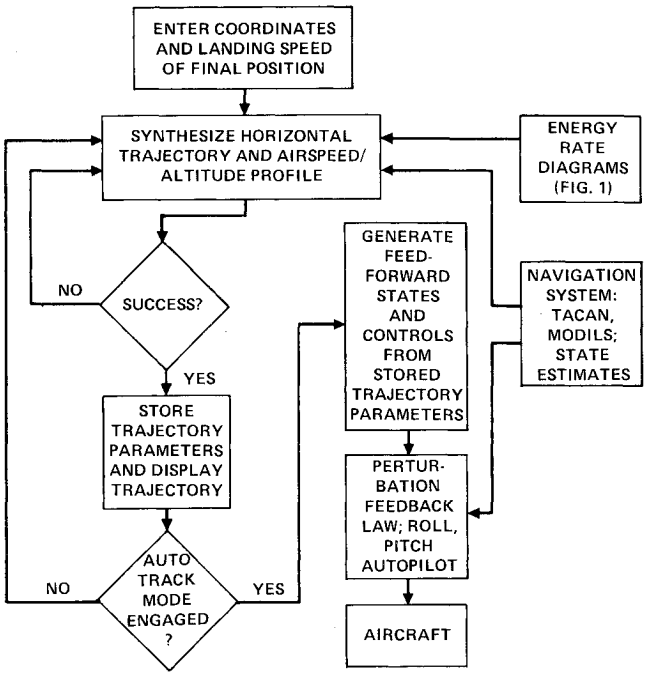

Fig. 7 Simplified flow diagram of guidance system.

where V_{ar} is in units of feet per second. Extensive computer calculations have verified that the closed-loop eigenvalues of this system have damping factors of 0.707 or greater and real parts less than -0.05/s at all operating points. These characteristics provide adequate tracking performance. When operating in region I of Fig. 6, the last row of K is set to zero since nozzle angle is not used for control. In regions II and III, throttle perturbations are limited to positive values, while in region II, nozzle perturbations are limited to positive values. In region IV, each control moves freely but negative throttle perturbations are limited to -2% rpm, as previously explained. Control limiting can reduce the effectiveness of integral feedback of speed and altitude. Some design considerations for these integral feedback loops are given in Ref. 9.

The throttle and nozzle angle perturbations generated by the control law will generally be of opposite sign, because the elements of the first row of K all have opposite sign of the third-row elements. Thus, even in region II, where throttle and nozzle perturbations are each limited to move only in the positive direction, they are not generally limited simultaneously. This implies that two controls, either throttle and pitch or nozzle and pitch, are free to move. Transient response studies using a nonlinear simulation of the aircraft and guidance system have shown that the control power is adequate to provide rapid and well-damped airspeed and altitude error responses in region II.

Guidance Algorithm Overview

A flow chart illustrating the integration of major functions within the guidance system is shown in Fig. 7. The pilot enters

$$K = \begin{bmatrix} \frac{-40}{V_{ar}} & \frac{-40}{V_{ar}} & \frac{-8}{V_{ar}} & \frac{-4\cos\nu_r}{V_{ar}} & \frac{-0.6}{V_{ar}} \\ 0 & -0.4 & \frac{-14}{V_{ar}} & 0 & \frac{-0.2}{V_{ar}} \\ 3 & 2 & 0.6 & 0.3 & 0.05 \max\left\{0, \frac{\delta_f - 45 \text{ deg}}{20}\right\} \end{bmatrix}$$

into the guidance computer the coordinates, altitude, and landing airspeed to be achieved at the desired final position on the approach path (see Fig. 3) or, alternatively, he selects a capture waypoint with prestored coordinates. Trajectory synthesis can begin after the navigation system has computed the current position and velocity components of the aircraft. The first step in the synthesis process involves computing the horizontal trajectory parameters using the technique described in the Appendix. This step is always successful. In the second step, the altitude and speed profile are synthesized using the energy rate diagram of Fig. 1 in conjunction with the logic described in the section on Synthesis of Complete Profiles. This step is not always successful. For example, if the horizontal path computed in the first step is very short and the differences in speed and altitude between initial and final aircraft positions are large, a flyable trajectory along that path may not exist. During synthesis, such a failure is detected as a negative cruise distance d_c in Eq. (12). A failure to synthesize is an unlikely event in landing approaches initiated several miles from the final point, the usual situation; if the failure occurs, however, the synthesis is repeated using updated position and velocity vectors, which aircraft motion has changed during the time the synthesis was in progress. The pilot can also fly the aircraft manually to a more favorable location (path stretching) for a successful synthesis.

After a trajectory has been successfully synthesized, its parameters are stored and the horizontal path is displayed to the pilot on a map-like cathode ray display (see Ref. 2 for details of this device). The appearance of the trajectory on the display is also a cue to the pilot that a valid trajectory has been successfully synthesized. The stored and displayed trajectory is refreshed by repeating the synthesis every few seconds until the pilot engages the auto track mode. At that time, the last synthesized trajectory is frozen and its reference states and controls are regenerated in real time. These reference values are fed forward to the perturbation feedback law, which causes the aircraft to track the synthesized trajectory. Three-dimensional navigation data for computing errors between the aircraft and the reference trajectory are obtained from TACAN (TACtical Air Navigation System) or MODILS (MODular Instrument Landing System, an experimental Microwave Landing System), with automatic switching to the most accurate signal.

It is important to note that once automatic tracking of a trajectory has begun, the stored trajectory is not refreshed, though this may be desirable if unmodeled wind or transients in navigation introduce large tracking errors. The real-time operating system has been configured to add this capability in future flight experiments. Also, a technique is incorporated in the flight software that compensates the trajectory for the changes in aircraft position occurring during the time (up to 6 s) the trajectory is synthesized.

Flight Test Results

Figure 8 shows the major portion of various time histories for a straight-in flight test approach starting 7 n.mi. from touchdown, at 3000 ft altitude and 140 knots. The deceleration at 0.03 g begins in level flight at point A, 4.7 n.mi. from touchdown. The descent begins at point B, 3.7 n.mi. from touchdown. The entire approach trajectory was flown using TACAN for navigation. The TACAN station was located at the airport a few hundred feet from the runway centerline. Because of its favorable location, the TACAN station provided sufficient navigation accuracy for flying the approach automatically to within a half-mile of touchdown without switching to the higher precision MODILS as would normally be required. There was light-to-moderate turbulence and an average headwind of about 15 knots below 4000 ft as measured by a radar tracked weather balloon just prior to takeoff. However, the wind profile was not entered into the synthesis logic and thus constituted an *unmodeled* wind. Altitude errors, except near the pitchdown point, did not

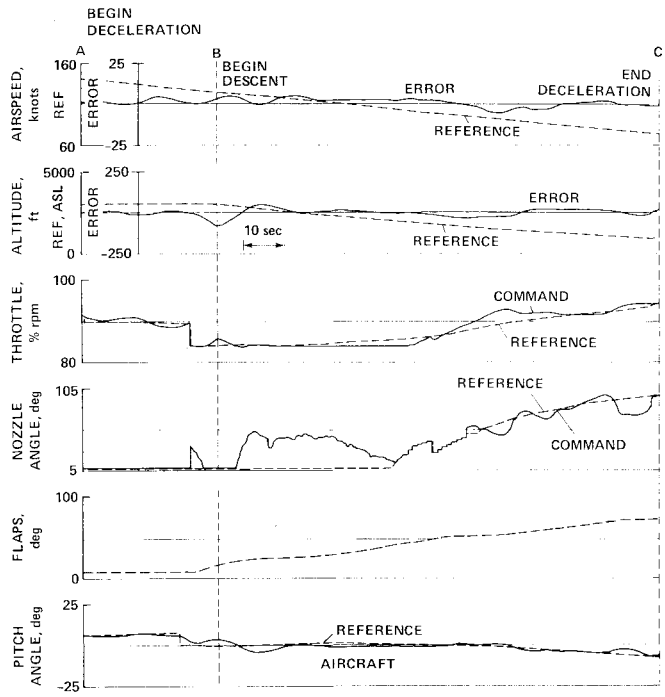

Fig. 8 Flight test results, straight-in approach, runway at 140 ft above sea level.

exceed 35 ft and decreased to about 15 ft near the end. Speed errors during deceleration were less than 10 ft/s, and decreased to about 1 ft/s at the end. If allowance is made for the presence of turbulence, winds, and navigation system noise during the flight, these errors agree reasonably well with simulation results and are acceptably low. The control perturbation biases, evidently caused by modeling errors and the unmodeled wind, are larger than those seen in simulation, though they are not excessive. Nozzle bias during the middle of the deceleration averages about 25 deg. While this seems large, it should be noted that during this interval the throttle is at flight idle, where the effect of nozzle on energy rate is a minimum. On the whole, the control biases represent fairly small errors in the energy rate model. The flight test results can, of course, be used to improve the accuracy of the energy rate model of the aircraft.

The crosstrack error at the end of deceleration, point C, 0.9 n.mi. from touchdown, was measured by precision radar as 80 ft. This error is an important criterion for determining how close point C can be placed to touchdown when navigating with TACAN. Pilots judged the action of the automatic control law as smooth and the trajectory synthesis technique as a convenient and effective tool for optimizing approach trajectories.

The fuel consumption of this automatically flown trajectory was compared with that of a trajectory flown by a test pilot under simulated instrument fligh rule conditions. In order to provide a basis for comparison, the manually flown trajectory began from the same initial distance-to-touchdown, airspeed, and altitude as the automatically flown trajectory. The approach was made with the aid of a flight director system which displayed to the pilot lateral and longitudinal deviations from a straight-in 7.5 deg approach path. The fuel used for the automatic approach was 381 lb, while that for the manually flown one was 500 lb. Further simulations and flight tests are in progress to compare the fuel consumption for various approach trajectories, flight director designs, and wind conditions.

Conclusions

The automatic guidance system described in this paper achieves the dual goal of fully automatic flight and near-optimal fuel conservation through the technique of fast-time

onboard trajectory synthesis. This technique overcomes the performance limitations inherent in a stored precalculated trajectory by adapting the trajectory to the unique conditions encountered in each landing approach. The ability to adapt is crucial in the terminal area since the initial conditions for starting the approach and the wind and temperature profiles are not predictable with sufficient accuracy prior to takeoff. Synthesized profiles always delay the start of the descent and deceleration points as much as possible. Flight evaluation using a powered-lift STOL aircraft showed that an automatically synthesized approach saves approximately 120 lb of fuel during the last 7 miles of the approach relative to one flown manually with only conventional flight director guidance. The design procedure described herein for a STOL aircraft is applicable with lesser computer complexity to conventional aircraft. The algorithm is also suitable for incorporating in advanced flight management systems currently under development by industry.

Appendix

This appendix derives the expressions for synthesizing horizontal capture trajectories for flying an aircraft from a given initial position and heading to a specified final position and heading. Figure 3 is used to explain the problem and define the variables. The turns are arcs of the circles shown in the figure and the straight portion of the trajectory must be a line tangent to both circles. Since the initial and final turns may be either clockwise or counterclockwise, there are four possible combinations of turning directions—two with the initial and final turns in the same direction, and two in opposite directions. Figure 3 illustrates one solution of each type. If a given pair of circles is entirely separate, i.e., no part of one circle lies within the other, it is possible to draw four tangent lines between the pair. However, vector $\bar{D}$ along the tangent line from the initial to the final circle coincides with the direction of rotation at both tangent points for only one of the four tangent lines as shown in the figure.

In the figure, the final position and the origin of the coordinate system are located on the runway centerline. However, the derivation is for arbitrary locations. Furthermore, all variables are defined so that the derivation applies to all possible combinations of turning directions.

Figure 3a is for the case where both turns are in the same direction and the tangent vector $\bar{D}$ does not cross $\bar{Q}$, while in Fig. 3b the turns are in opposite directions and $\bar{D}$ crosses $\bar{Q}$. Initially, the aircraft is at (X_i, Y_i) in some inertial Cartesian coordinate system with heading H_i defined as positive clockwise from the X axis, and $\bar{v}_1$ is a unit vector in the direction of the velocity. The vector distance from (X_i, Y_i) to the center of the turn is given by $\bar{u}_1 R_1$, where R_1 is the radius of turn and $\bar{u}_1$ a unit vector normal to $\bar{v}_1$ and positive to the right of $\bar{v}_1$. Therefore, the vector from (X_i, Y_i) to the center (XC_1, YC_1) is $R_1\bar{u}_1$ for a right turn and $-R_1\bar{u}_1$ for a left turn. The directions of turn are accounted for by writing the radius vector as $R_1S_1\bar{u}_1$, where $S_1 = +1.0$ for right turns and $S_1 = -1.0$ for left turns. Similarly, the direction of the final turn is denoted by S_2.

The aircraft moves along the circle from (X_i, Y_i) to the tangent point (X_2, Y_2) which has a radius vector $R_1S_1\bar{u}_2$. The tangent vector from (X_2, Y_2) at the end of the initial turn to (X_3, Y_3) at the beginning of the final turn is $\bar{D}$. The radius vector at (X_3, Y_3) is $R_2S_2\bar{u}_3$, but since $\bar{u}_2$ and $\bar{u}_3$ must be normal to $\bar{D}$, $\bar{u}_2 = \bar{u}_3$. Likewise, the headings H_2 and H_3 at the two tangent points are equal. The final turn ends at (X_f, Y_f) with heading H_f and radius vector $R_2S_2\bar{u}_4$.

Using this notation, we can write

$$\bar{D} + R_2\bar{u}_2S_2 = R_1\bar{u}_2S_1 + \bar{Q}$$

or

$$\bar{Q} = \bar{D} + \bar{u}_2(R_2S_2 - R_1S_1) \tag{A1}$$

and therefore, since $\bar{D}$ and $\bar{u}_2$ are perpendicular,

$$D \equiv |\bar{D}| = \sqrt{Q^2 - (R_2S_2 - R_1S_1)^2} \tag{A2}$$

where, by definition,

$$Q \equiv |\bar{Q}| = \sqrt{(XC_2 - XC_1)^2 + (YC_2 - YC_1)^2} \tag{A3}$$

It can be seen from Eq. (A2) that no real solution exists if $Q < |R_2S_2 - R_1S_1|$. When the turns are in opposite directions, $S_1 = -S_2$, and there is no real solution for $Q < (R_1 + R_2)$, i.e., if the circles intersect. On the other hand, for rotations in the same directions, $S_1 = S_2$ and a real solution exists unless $Q < |R_2 - R_1|$, i.e., unless one circle lies entirely within the other. From geometric construction it can be shown that there always exist at least two real solutions. From the definition of the radius vectors, one can write for the real solutions:

$$R_1\bar{u}_1S_1 = \begin{pmatrix} -R_1S_1\sin H_i \\ R_1S_1\cos H_i \end{pmatrix} \tag{A4}$$

and

$$R_1\bar{u}_1S_1 = \begin{pmatrix} XC_1 - X_i \\ YC_1 - Y_i \end{pmatrix} \tag{A5}$$

Equating Eqs. (A4) and (A5) gives

$$XC_1 = X_1 - R_1S_1\sin H_i \qquad YC_1 = Y_1 + R_1S_1\cos H_i \tag{A6}$$

Similarly,

$$XC_2 = X_f - R_2S_2\sin H_f \qquad YC_2 = Y_f - R_2S_2\cos H_f \tag{A7}$$

The radius vectors at the tangent points can be used in the same manner to compute the components of $\bar{X}_2$ and $\bar{X}_3$

$$X_2 = XC_1 + R_1S_1\sin H_2 \tag{A8a}$$

$$Y_2 = YC_1 - R_1S_1\cos H_2 \tag{A8b}$$

$$X_3 = XC_2 + R_2S_2\sin H_2 \tag{A9a}$$

$$Y_3 = YC_2 - R_2S_2\cos H_2 \tag{A9b}$$

Subtracting Eq. (A8a) from (A9a) and Eq. (A8b) from (A9b) gives the components of $\bar{D}$:

$$\begin{aligned} X_3 - X_2 &= XC_2 - XC_1 + (R_2S_2 - R_1S_1)\sin H_2 \\ Y_3 - Y_2 &= YC_2 - YC_1 - (R_2S_2 - R_1S_1)\cos H_2 \end{aligned} \tag{A10}$$

Another expression for the components of $\bar{D}$ is:

$$X_3 - X_2 = D\cos H_2 \qquad Y_3 - Y_2 = D\sin H_2 \tag{A11}$$

Equating the corresponding pairs in Eqs. (A10) and (A11) gives

$$\begin{aligned} D\cos H_2 &= (XC_2 - XC_1) + (R_2S_2 - R_1S_1)\sin H_2 \\ D\sin H_2 &= (YC_2 - YC_1) - (R_2S_2 - R_1S_1)\cos H_2 \end{aligned} \tag{A12}$$

Equations (A12) can be solved for the tangent of H_2:

$$\tan H_2 = \frac{(YC_2 - YC_1)D - (R_2S_2 - R_1S_1)(XC_2 - XC_1)}{(XC_2 - XC_1)D + (R_2S_2 - R_1S_1)(YC_2 - YC_1)} \tag{A13}$$

Equations (A6-A9) and (A13) completely specify a capture trajectory for any combination of S_1 and S_2. However, the length of the trajectory is also needed in order to determine which of the feasible trajectories gives the minimum distance. The first turn angle is

$$TR_1 = (H_2 - H_i) + 2\pi C_1 S_1$$

where

$$C_1 = \begin{cases} 0 & \text{if } S_1(H_2 - H_i) \geq 0 \\ 1 & \text{if } S_1(H_2 - H_i) < 0 \end{cases} \quad \text{(A14)}$$

and the second turn angle is

$$TR_2 = (H_f - H_2) + 2\pi C_2 S$$

where

$$C_2 = \begin{cases} 0 & \text{if } S_2(H_f - H_2) \geq 0 \\ 1 & \text{if } S_2(H_f - H_2) < 0 \end{cases} \quad \text{(A15)}$$

Finally, the total length of the capture path is

$$d_h = |\bar{D}| + R_1 |TR_1| + R_2 |TR_2| \quad \text{(A16)}$$

The algorithm computes the length of trajectories for all feasible pairs of S_1 and S_2 and then picks the shortest length trajectory. A FORTRAN listing and additional details of this algorithm, including captures with three turns, can be found in Ref. 10.

References

[1] Neuman, F., Watson, D.M., and Bradbury, P., "Operational Description of an Experimental Digital Avionics System for STOL Airplanes," NASA TM X-62,448, Dec. 1975.

[2] Lee, H.Q., Neuman, F., and Hardy, G.G., "4-D Area Navigation System Description and Flight Tests," NASA TN D-7874, Aug. 1975.

[3] Byrson, A.E. Jr., Desai, M.N., and Hoffman, W.C., "Energy State Approximation in Performance Optimization of Supersonic Aircraft," *Journal of Aircraft*, Vol. 6, Nov.-Dec. 1969, pp. 481-487.

[4] Erzberger, H. and Lee, H.Q., "Terminal-Area Guidance Algorithms for Automated Air Traffic Control," NASA TN D-6773, April 1972.

[5] Pecsvaradi, T., "Four-Dimensional Guidance Algorithms for Aircraft in an Air Traffic Control Environment," NASA TN D-7829, March 1975.

[6] Erzberger, H., McLean, J.D., and Barman, J.F., "Fixed-Range Optimum Trajectories for Short-Haul Aircraft," NASA TN D-8115, Dec. 1975.

[7] Jakob, H., "An Engineering Optimization Method with Application to STOL Aircraft Approach and Landing Trajectories," NASA TN D-6978, Sept. 1972.

[8] Bryson, A.E. Jr. and Ho, Y.C., *Applied Optimal Control*, Blaisdell Publishing Co., Waltham, Mass., 1969, pp. 148-176.

[9] Slater, G., "Analysis of Integral Controls in Linear Quadratic Regulator Design," AIAA Paper 79-1743, *Proceedings of the AIAA Guidance and Control Conference*, Boulder, Colo, Aug. 6-8, 1979.

[10] McLean, J.D., "A New Algorithm for Horizontal Capture Trajectories," NASA TM-81186, March 1980.